Bulletin of the Seismological Society of America, Vol. 93, No. 3, pp. 1333–1344, June 2003

Ⓔ

A Structural Interpretation of the Aftershock "Cloud" of the 1992 M_w 7.3 Landers Earthquake

by Jing Liu, Kerry Sieh, and Egill Hauksson

Abstract We analyze the spatial relationship of relocated aftershocks to the principal rupture planes of the M_w 7.3 1992 Landers mainshock from a structural point of view. We find that the aftershocks constitute primarily a several-kilometer-wide damage zone centered on the mainshock rupture planes. The intensity of damage decreases away from the principal faults. Less than half of the aftershocks occurred within 1 km of the mainshock planes, and perhaps only 5% of the aftershocks are candidates for rerupture of the mainshock faults. Moreover, it seems that aftershocks along the Landers rupture have *b*-values that correlate well with the complexity of the mainshock rupture. Low *b*-values occur along segments that are simple, whereas higher *b*-values correlate with sections that are more complex. Thus, structural complexity appears to correlate with a greater relative abundance of small earthquakes. These observations imply that aftershock populations reflect fault populations in the medium surrounding the principal faults rather than the behavior of the mainshock planes themselves.

Online material: Arcview information about the surface rupture of the Landers mainshock.

Introduction

Aftershock sequences of moderate to large crustal earthquakes provide information about rupture processes of fault zones. Their spatial and temporal distributions have been exploited to understand better their relationship to mainshocks. Previous studies show that aftershocks generally form a "cloud" around the principal fault ruptures (e.g., Mendoza and Hartzell, 1988). However, location errors often result in uncertainties as to whether the aftershocks occur on the fault that slipped to produce the mainshock or within the volumes on either side of the rupture surface.

Aftershocks are often considered, either implicitly or explicitly, to have occurred on the mainshock rupture plane. For instance, aftershock hypocenters are widely used to identify the length, depth, dip, and geometric complexities of the mainshock rupture (e.g., Kanamori and Anderson, 1975; Fehler and Johnson, 1989; Dietz and Ellsworth, 1990; Nakamura and Ando, 1996; Shaw and Shearer, 1999; Rubin and Gillard, 2000). For these purposes, aftershock hypocenters are assumed to occur on (or at least very near) the mainshock rupture planes. Recent improvements in location accuracy generally support this assumption, in that they commonly show a reduction in the dimension of the aftershock cloud perpendicular to the principal fault planes (Richards-Dinger and Shearer, 2000; Waldhauser and Ellsworth, 2000).

However, there is reason to suspect that most aftershock hypocenters are not, in fact, located on the mainshock rupture plane. Instead, aftershocks form a zone or cloud surrounding the mainshock rupture. For example, evidence has accumulated in support of the notion that stress changes and viscous flow in the lower crust induced by the mainshock rupture trigger off-plane aftershocks, even at great distances from the mainshock rupture plane (e.g., Das and Scholz, 1981; Stein and Lisowski, 1983; Reasenberg and Simpson, 1992; King *et al.*, 1994; Stein *et al.*, 1994; Hill *et al.*, 1995; Gomberg and Davis, 1996; Deng *et al.*, 1998, 1999; Hardebeck *et al.*, 1998).

One question that has seldom been asked is, What do aftershocks tell us about the geologic structure of fault zones that produce large earthquakes? Their almost universal association with large crustal earthquakes suggests that they must be caused by the stress perturbations induced by the mainshock rupture. But are they reruptures of the mainshock plane, or are they the result of subsidiary faulting in the fault blocks that bound the primary fault? If the latter is true, then aftershocks constitute a structural damage zone around the mainshock ruptures, perhaps reflecting the zone of lesser fracturing around the principal rupture that one commonly sees in a geologic outcrop. The answer to this question has an important bearing on the physics of earthquake faulting. For example, it could help resolve whether irregularities in slip distribution, such as those suggested by seismologic and

geodetic inversions (Kanamori *et al.*, 1992; Hudnut *et al.*, 1994; Wald and Heaton, 1994), are smoothed out by rerupture during aftershocks.

In this article, we present a detailed analysis of the 1992 Landers earthquake sequence to clarify the relationship of aftershock distribution to mainshock rupture from a structural point of view. The 1992 Landers aftershocks are an exceptionally well-recorded sequence. They afford an excellent opportunity to answer the aforementioned questions because (1) a detailed map of surface rupture places unambiguous constraints on both the location of the rupture plane and a variety of geometric complexities, (2) hundreds of slip measurements constrain the sense and magnitude of fault slip, and (3) there are tens of thousands of aftershocks, with location errors of less than 1 km. Unlike previous studies of the Landers aftershock sequence (e.g., Wiemer and Katsumata, 1999), we demonstrate a link between aftershocks and the geologic structure of the fault zones.

Data

Surface Rupture

The surface rupture of the Landers mainshock that we use (Fig. 1) is a compilation of the detailed mapping of several groups. (Ⓔ Arcview files are available online at the SSA web site.) To produce this database, the surface ruptures were mapped onto 1:6000-scale postrupture aerial photos in the field during the weeks immediately following the Landers earthquake (Sieh *et al.*, 1993). The results of this mapping were then compiled onto 1:24,000 U.S. Geological Survey (USGS) topographic maps, which had been enlarged to the same scale. Surface ruptures were mapped in greatest detail along the northernmost 35 km of the rupture. This section of the rupture includes the Camp Rock fault, the Emerson fault (McGill and Rubin, 1999), the step-over between the Emerson and Homestead Valley faults (Zachariasen and Sieh, 1995), and a 3-km-long slip gap at the northern end of the step-over between the Homestead Valley and Johnson Valley faults (Spotila and Sieh, 1995) (segments 1, 2, 3, 4, and 6 in Fig. 1). The southern one-third of the rupture, although mapped in detail by USGS and California Department of Conservation, Division of Mines and Geology, personnel (CDMG) (USGS/CDMG, 1992; CDMG, 2000); is not shown in as much detail, but the location of the main surface rupture zones are in the database.

Aftershocks

We use the relocated aftershock hypocenters of Hauksson (2000) and Richards-Dinger and Shearer (2000). Hauksson (2000) used 3D raytracing techniques as well as a 3D crustal velocity model of southern California that was an improvement over the one used to create the catalog locations. For his relocations, explosions set off for earlier trapped-mode studies provided the calibration for absolute locations. These new locations have average 1σ errors of 0.35 km in the horizontal and 0.88 km in the vertical dimension (Fig. 2). We used only the 29,399 aftershocks that have horizontal and vertical location errors no greater than 1 km and 1.5 km, respectively, and that occurred in the period from 28 June 1992 to 22 May 1998. We also repeated our analysis using Richards-Dinger and Shearer's (2000) relocations. Their relocation was done by an L1-norm, grid-search approach on a smooth 1D velocity model, plus a refining source-specific station term correction. Their relocations have median horizontal and vertical location errors of 0.31 and 0.75 km, respectively.

Observations

The Aftershocks Occur in a Vertically Dipping Cloud

Figure 3 shows that the Landers aftershocks extend far into the regions surrounding the coseismic rupture planes. Note that the contour representing a density of 5–45 events/km^2 commonly extends 3–8 km from the mapped surface ruptures, distances far greater than the uncertainty in aftershock locations. Also, near the mainshock rupture, aftershocks cluster locally at fault termini and step-overs. For instance, the Johnson Valley–Homestead Valley step-over has the highest aftershock density of the entire sequence: up to 585 events/km^2. Another unusually high concentration occurs at the southern end of the Johnson Valley fault. Another cluster, in the middle of the Johnson Valley fault, is associated with a minor fault splay.

The scatter we see is not the result of viewing a dipping band of aftershocks in plan view. Figure 4 shows that the aftershock clouds dip vertically (or nearly so). Furthermore, they do not reflect dipping mainshock fault ruptures, because the clouds do not spread out just to one side of the principal ruptures. Rather, they occur on both sides of the surfacial ruptures (Fig. 3).

To facilitate the examination of the distributions of the aftershocks, we divide the Landers rupture into nine sections from north to south and inspect the distribution of $M \geq 2$ aftershock hypocenters in nine cross-sectional views perpendicular to the Landers fault zone (Figs. 1 and 4). Along the Camp Rock fault (section 1), aftershocks are too few to delineate a volume surrounding the principal fault. But along the Emerson fault (sections 2 and 3), aftershocks define a nearly vertically dipping planar structure that is aligned with the surface trace of the Emerson fault and a broad diffuse zone to the east of the fault. The cloud along the Homestead Valley fault (sections 4 and 5) is relatively broad and roughly vertical. In the region of the Homestead Valley–Johnson Valley fault step-over (section 6), the aftershock cloud is particularly intense and is a 3-km-wide vertical band, particularly well expressed at depths between 5 and 13 km. Across the Johnson Valley fault (section 7), the 1- to 2-km-wide aftershock zone sharply delineates the mainshock fault plane. Although a surface rupture and surface fault are absent in the gap between the Johnson Valley and Eureka Peak

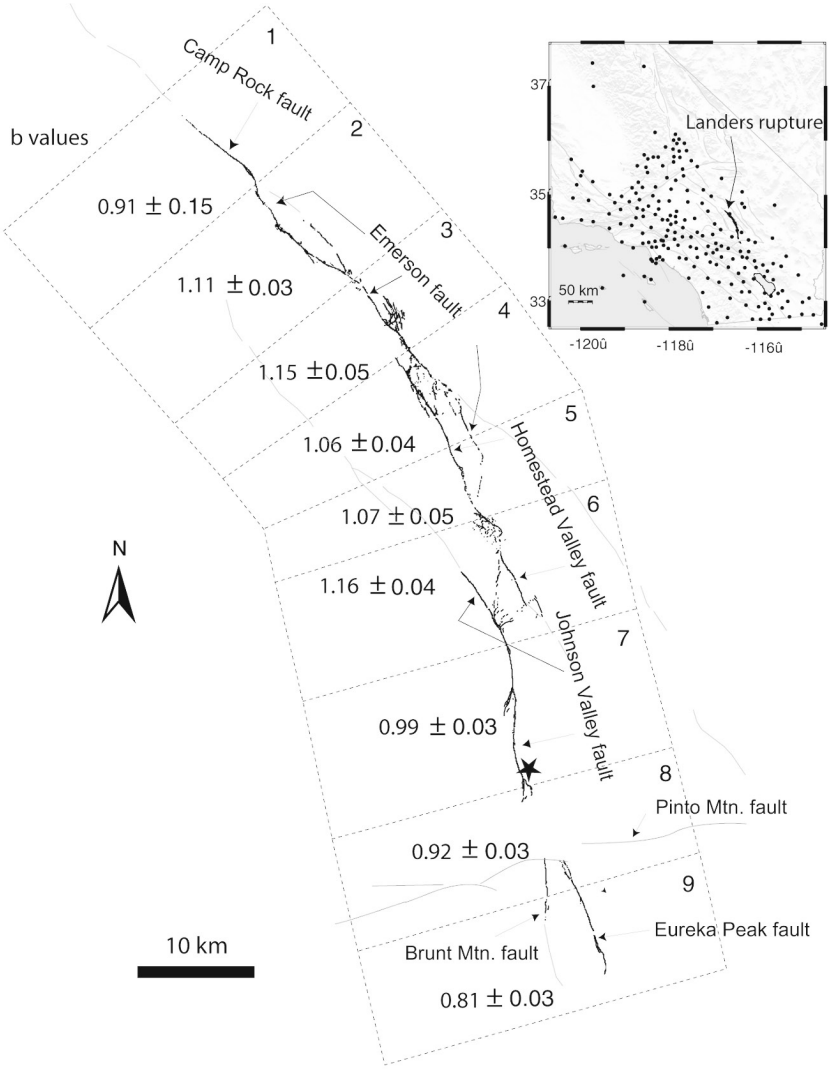

Figure 1. Map of the surficial ruptures of the 1992 Landers earthquake. The rupture is divided into nine sections for an examination of aftershock locations in cross-sectional views. Aftershock *b*-values in these sections range from about 0.8 to 1.2. Sections in which the rupture is simple have lower *b*-values, and sections of complex rupture have higher *b*-values. The inset figure shows the distribution of seismographic stations during the period of the Landers aftershock sequence used in this article.

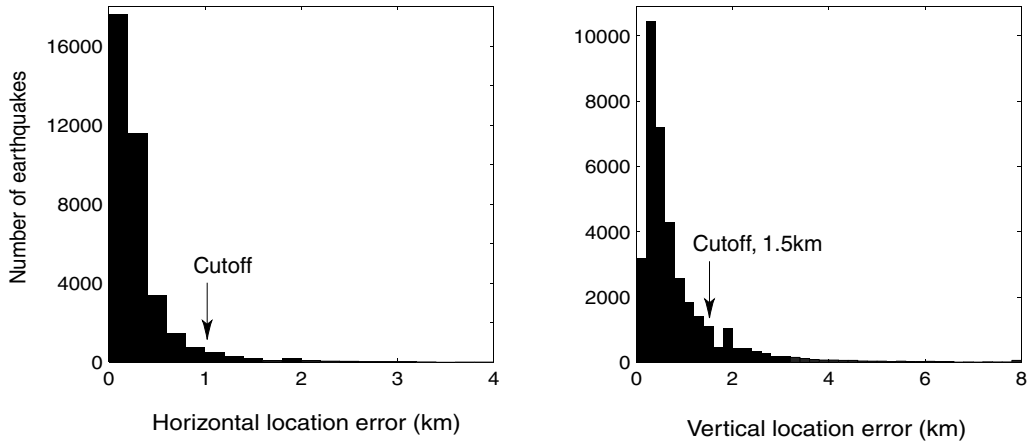

Figure 2. Histograms of horizontal and vertical location errors of relocated 1992 Landers aftershocks from 28 June 1992 to 22 May 1998. Relocations by Hauksson (2000). We excluded aftershocks with location errors greater than 1 km in the horizontal and 1.5 km in the vertical to avoid the use of ill-located aftershocks in our analysis.

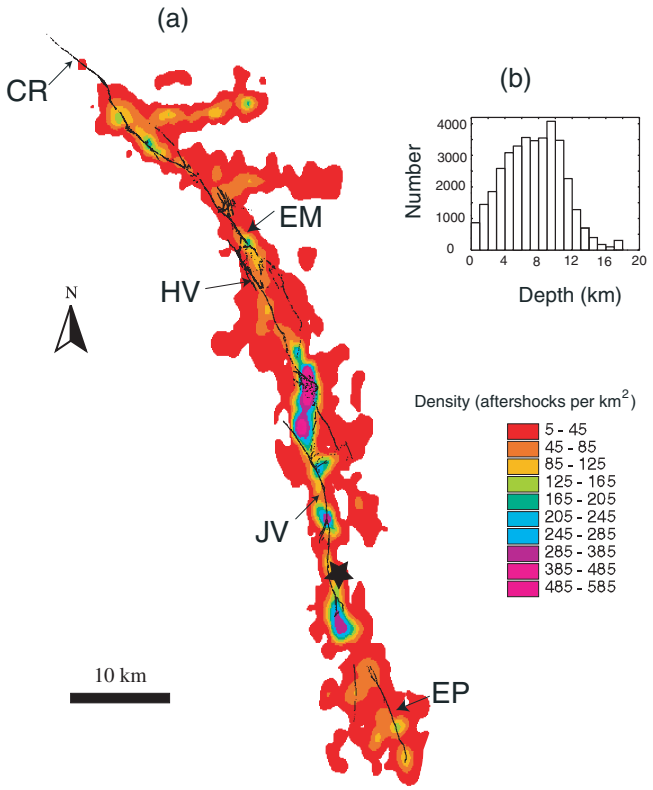

Figure 3. (a) Map view of the surficial ruptures of the 1992 Landers earthquake and aftershock density distribution. The contour representing a density of 5–45 events/km^2 commonly extends 3–8 km from the principal ruptures, distances far greater than the uncertainty in aftershock locations. A star marks the location of the mainshock epicenter. Abbreviations are CR, Camp Rock fault; EM, Emerson fault; HV, Homestead Valley fault; JV, Johnson Valley fault; EP, Eureka Peak fault. (b) Histogram of aftershocks as a function of depth.

faults (section 8), aftershocks form a well-defined vertically elongate cluster. The most scattered aftershock zone occurs across the Eureka Peak fault section (section 9).

Most Aftershocks Occur off the Mainshock Fault Planes

Overall, the vertical dip of the aftershock clouds and their symmetry about the mainshock ruptures suggest strongly that the mainshock faults dip vertically. This interpretation is consistent with the focal mechanism of the Landers mainshock (Kanamori *et al.*, 1992; Hauksson *et al.*, 1993). Now that we are confident that the mainshock rupture planes are vertical or nearly so, we may proceed to estimate how many aftershocks might have occurred on the mainshock planes.

The mainshock fault planes include two parts: those that ruptured during the mainshock and those that did not. We simplify the mapped surface ruptures as references to the parts of faults that failed in the mainshock. The modification is made mainly by fitting straight lines through the alignments of en echelon cracks; the lengths of fitted lines vary depending on how straight the en echelon cracks are aligned. But if the cracks extend no more than 500 m, such as those in the step-over between the Homestead Valley fault and Emerson fault, we choose to ignore them. Nonetheless, the simplified faults match closely with the mapped ruptures (Fig. 5). Another major modification is made at the 4.5-km-long section immediately north of the step-over between the Homestead Valley fault and Johnson Valley fault, where surface ruptures were reportedly northward thrust faults at shallow depth (Spotila and Sieh, 1995). There, we consider that the Homestead Valley fault at depth has the same orientation as that outside the structure knot.

We also consider faults beyond the ends of the rupture because a large earthquake sometimes does not rupture the entirety of a fault and aftershocks can still fall on the fault plane in the portions outside the bounds of the mainshock rupture. Parts of four major faults that did not break in the 1992 Landers earthquake are shown in Figure 5 as thin lines; these include the northern half of the Camp Rock fault, the southern two-thirds of the Emerson fault, the northern two-thirds of the Johnson Valley fault, and the southern end of the Homestead Valley fault (Jennings, 1994; CDMG, 2000).

Figure 6a shows how both the number of Landers aftershocks and the moment for 0.5-km-wide bins vary as a function of distance from the surface traces of the mainshock fault planes defined in Figure 5. Both the numbers of aftershocks and moment attenuate symmetrically out from the principal fault planes. This fault-normal distribution is independent of the time period sampled. For example, the ratios of near-fault to total aftershocks are similar for the periods encompassing 6 months and 6 years after the mainshock (Table 1). The distributions are not sensitive to the choice of minimum magnitude cutoff ($M_L \geq 0$ or $M_L \geq 2$) or location method either. Use of the Richards-Dinger and Shearer (2000) catalog yields similar results (Table 1). Relocations using a double difference method (Hauksson and Michael, 2001) do not change the results significantly, either.

The distributions of moment and number of events in Figure 6 indicate that the majority of aftershocks resulted from fault rupture well away from the principal fault planes. Only about 40% of the aftershocks occurred within 0.5 km of the main fault zone, the approximate uncertainty in horizontal location; but about 60%–65% occurred within 1 km of the mainshock fault zone (Table 1). A slightly more rigorous determination of those aftershocks that would be candidates for rerupture appears in Figure 6b. It yields a similar result. There, we consider the location error distribution normal to the faults. If we shift all aftershocks toward the nearest mainshock rupture by the amount of their 2σ location errors, we find a conservative upper bound to the number of

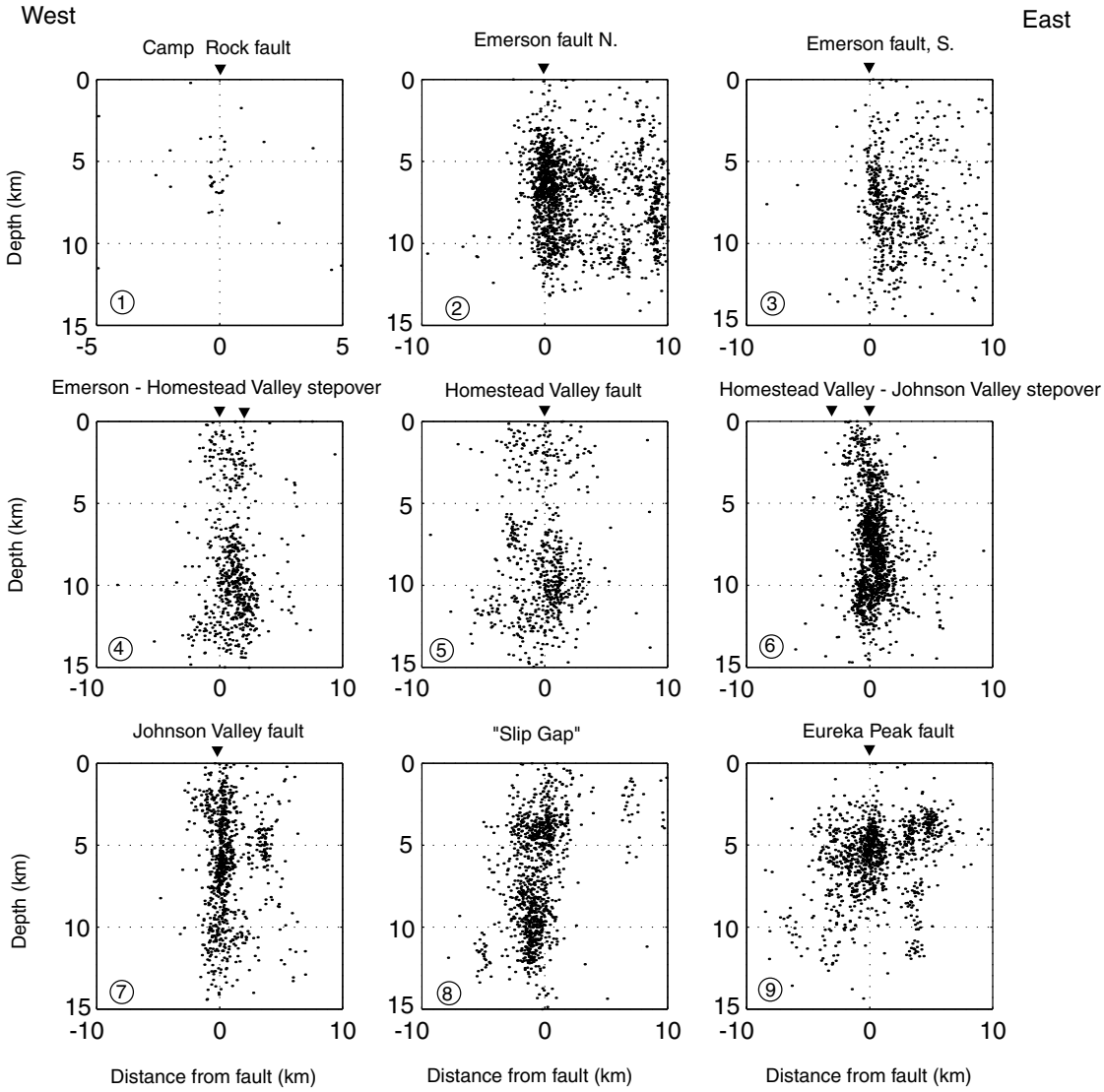

Figure 4. Cross-sectional views of aftershock locations ($M_L \geq 2$) for the nine sections shown in Figure 1. The inverted solid triangles denote traces of the principal mainshock ruptures. Aftershock clouds suggest nearly vertically dipping mainshock fault planes, because the clouds do not spread out just to one side of the principal ruptures.

aftershocks that might have occurred on the mainshock faults. These aftershocks are those between the two diagonal dashed lines in the figure. They constitute about 44% of aftershocks with $M \geq 0$.

Among the aftershocks that occurred within half a kilometer of the main fault zone and that are candidates of rerupture of mainshock fault planes, only about 1%–2% of the total aftershocks fell beyond the rupture ends on the Camp Rock fault, the Emerson fault, the Homestead Valley fault, and the Johnson Valley fault. This is in contrast with Rubin and Gillard's (2000) studies of the microearthquakes in the central San Andreas fault, where they found that the majority of aftershocks occurred on the mainshock fault plane, but beyond the termini of the mainshock rupture.

Aftershock Focal Mechanisms further Limit Which Aftershocks Can Represent Rerupture of the Mainshock Fault Planes

The Landers aftershocks have diverse focal mechanisms (Hauksson, 1994; Hardebeck *et al.*, 1998). This further constrains the number of aftershocks that are candidates for rerupture of the mainshock ruptures, since slip along most of the mainshock ruptures was principally right lateral. First-motion lower hemisphere focal mechanisms of the relocated aftershocks are determined for events that had 12 or more first motions. We use the grid-searching algorithm and computer programs by Reasenberg and Oppenheimer (1985). Since the first-motion solutions do not decide on which of the two planes, in our analysis we choose the plane with

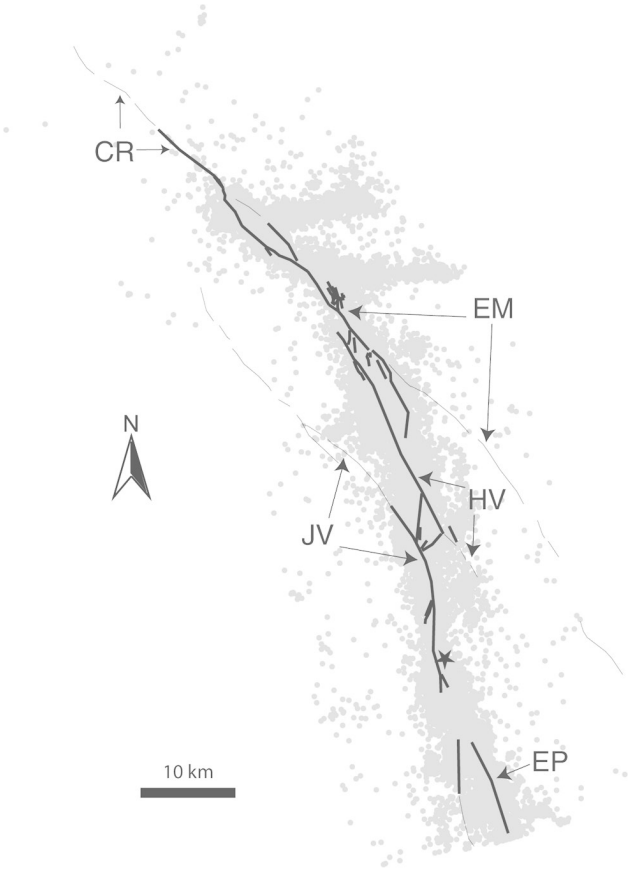

Figure 5. Map view of the surface traces of the mainshock fault planes and aftershock locations. Simplified surface ruptures, shown as thick lines, represent the fault planes that failed during the mainshock; fault planes beyond the ends of the mainshock ruptures are shown as thin lines. Abbreviations of the faults are the same as in Figure 3.

either a right-lateral component or pure vertical sense of motion.

Out of the 751 aftershocks that originated within half a kilometer of mainshock ruptures and have reliable first-motion solutions with the 90% confidence range of less than 60° in strike, only 25% have a focal plane with a right-lateral component of motion that is within 20° of the strike of the local mainshock rupture plane (Fig. 7a). However, only about half of the aftershocks have a dominant horizontal component of motion on the chosen plane (Fig. 7b), whereas the mainshock rupture was predominantly right lateral. Even within the step-overs, the right-lateral component of the mainshock rupture was larger than the vertical component (Spotila and Sieh, 1995; Zachariasen and Sieh, 1995). The focal mechanism statistics within 1 km of the main fault zone are nearly identical. Out of the 1225 aftershocks that occurred within 1 km of the mainshock ruptures and that satisfy the same criteria as above, 26% are within 20° of the strike of the local mainshock rupture plane, but half of these aftershocks do not have a right-lateral focal mechanism.

This suggests that of all 11,564 aftershocks with hypocenters within half a kilometer of the mainshock rupture plane, far fewer than half were produced by shear in directions consistent with the mainshock rupture. Taking proximity to the mainshock rupture and consistency of focal mechanism together, no more than about 15% of the total population of aftershocks are strong candidates for rerupture of the mainshock ruptures.

Aftershock *b*-Values Correlate with Mainshock Fault Complexity

The relationship between mainshock rupture geometry and aftershocks is also manifest in the correlation of *b*-values of the aftershock sequence and mainshock rupture complexity. To calculate *b*-values and their uncertainties in each of the nine volumes outlined in Figure 1, we used the maximum likelihood method of Aki (1965). The *b*-value for aftershocks with $M \geq 2.0$ appears in Figure 1 within each of the nine rectangles.

Aftershock *b*-values range along strike from about 0.8 to 1.2 and vary with the complexity of the mainshock rupture. Low *b*-values occur in sections where the rupture is the simplest, specifically along the southern third of the rupture (Johnson Valley and Eureka Peak faults) and along the northernmost segment (Camp Rock fault). The slip gap between the Johnson Valley and Eureka Peak fault, where no surface rupture was found, also has low *b*-values. The sections 12–50 km north of the mainshock epicenter, where the mainshock rupture was geometrically more complex than elsewhere (as evidenced by more minor faults and branches and a wider rupture zone), have high *b*-values. This correlation is consistent with previous observations that greater material heterogeneity and crack density correlate with higher *b*-values (Mogi, 1962; Mori and Abercrombie, 1997). Although we show here the *b*-values with a lower cutoff magnitude of *M* 2, repeated analysis shows that the spatial pattern in *b*-values between sections is independent of choices of magnitude cutoff. Moreover, these spatial variations in *b*-value agree with the results of Wiemer and Katsumata (1999), who found that *b*-values are high along the northern section ($b > 1.2$) and low on the southern section ($b < 0.9$) of the Landers rupture. They concluded that lower *b*-values resulted from lesser mainshock slip (Wiemer and Katsumata, 1999). Although this correlation is true for sections 1, 8, and 9, it is not true for section 7.

Discussion

All three sets of observations lead us to suspect that the Landers aftershocks are manifestations of a broad structural damage zone astride the mainshock faults. The width of the aftershock zone, the increase in aftershock moment release as one approaches the mainshock ruptures, and the correlation of *b*-values with fault complexity are all consistent with what one commonly sees in exposures of natural fault zones.

Exposures of large natural faults commonly consist of

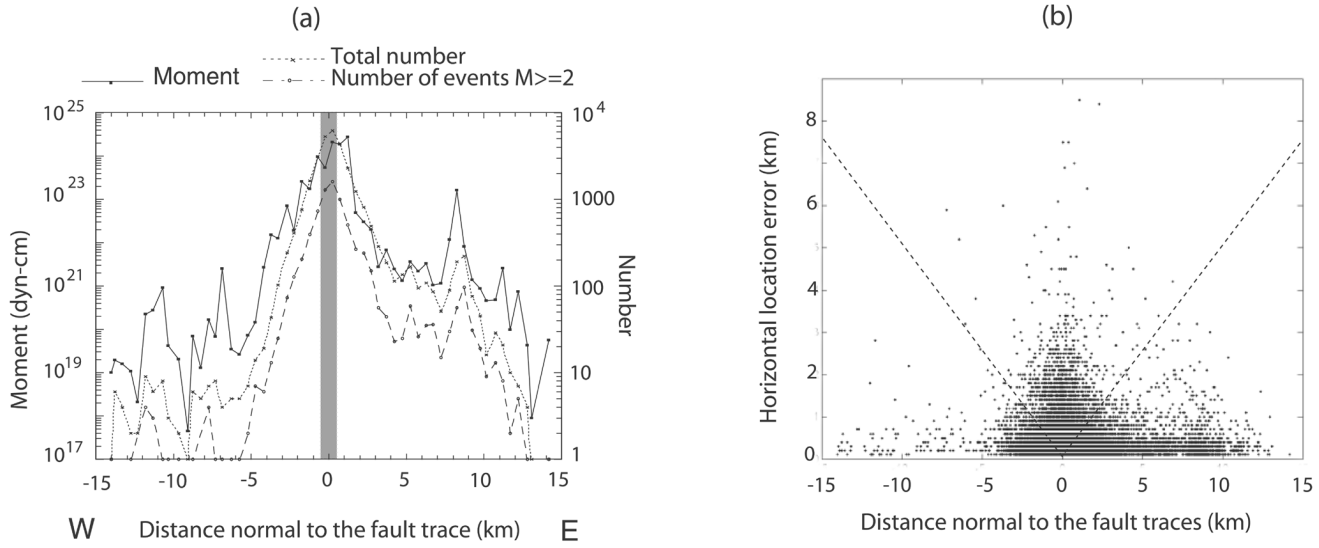

Figure 6. (a) Distributions of Landers aftershocks and (b) their horizontal location errors as a function of distance normal to the mainshock faults as shown in Figure 5, using relocated data set by Hauksson (2000). Only about 40% of the aftershocks occurred within 0.5 km of the mainshock faults. If we shift all aftershocks toward the nearest mainshock faults by the amounts of their 2σ location uncertainties, 44% of aftershocks might have occurred on the faults (those between the two diagonal dashed lines in Fig. 6b).

Table 1
Ratios of Near-Fault to the Total Population of Aftershocks during Different Time Periods

	Data Source	Time Period (mm/dd/yy–mm/dd/yy)	Number of Earthquakes $M_L \geq 0$	Number of Earthquakes $M_L \geq 2$	Summed Moment
Within 0.5 km of the mainshock fault planes	Hauksson (2000)	06/28/92–05/28/98	0.40	0.40	0.29
		06/28/92–12/31/92	0.41	0.41	0.30
	Richards-Dinger and Shearer (2000)	06/28/92–03/18/98	0.36	0.35	0.56 [0.36]
		06/28/92–12/31/92	0.36	0.36	0.63 [0.38]
Within 1 km of the mainshock fault planes	Hauksson (2000)	06/28/92–05/28/98	0.65	0.64	0.60
		06/28/92–12/31/92	0.64	0.64	0.62
	Richards-Dinger and Shearer (2000)	06/28/92–03/18/98	0.62	0.61	0.77
		06/28/92–12/31/92	0.61	0.61	0.85

Mainshock faults are defined in Figure 5. The ratios of summed moment from Richards-Dinger and Shearer's (2000) data set are higher because an *M* 5.7 aftershock is excluded in the analysis due to its large location uncertainty. If we include this event, the ratios shown in brackets are comparable to those from Hauksson (2000).

a narrow band of intensely sheared material (a gouge layer) surrounded by a broad swath of subsidiary faults (a damage zone) (Fig. 8; Chester and Logan, 1986; Wallace and Morris, 1986). The broader swath of damage commonly displays a progressive decrease in deformation intensity away from the principal fault, and the transition from the fault zone to undeformed host rock is gradual (Fig. 8; Chester and Logan, 1986; Wallace and Morris, 1986). Chester and Logan (1986) documented that fracture density in the damage zone generally decreases with distance away from the fault surface (Fig. 9a).

Aftershock sequences may provide exceptional opportunities to quantify strain distribution across crustal fault zones, information that is exceedingly difficult to obtain from the outcrop. The gouge layer–damage zone morphology of fault zones indicates that most of the displacement is accommodated within the gouge layer, supplemented by distributed cataclasis in the surrounding region (Chester and Logan, 1986; Chester *et al.*, 1993; Chester and Chester, 1998; Schulz and Evans, 1998). But it is difficult to evaluate quantitatively the strain distribution across a fault zone in outcrop, because reference features that can be traced across

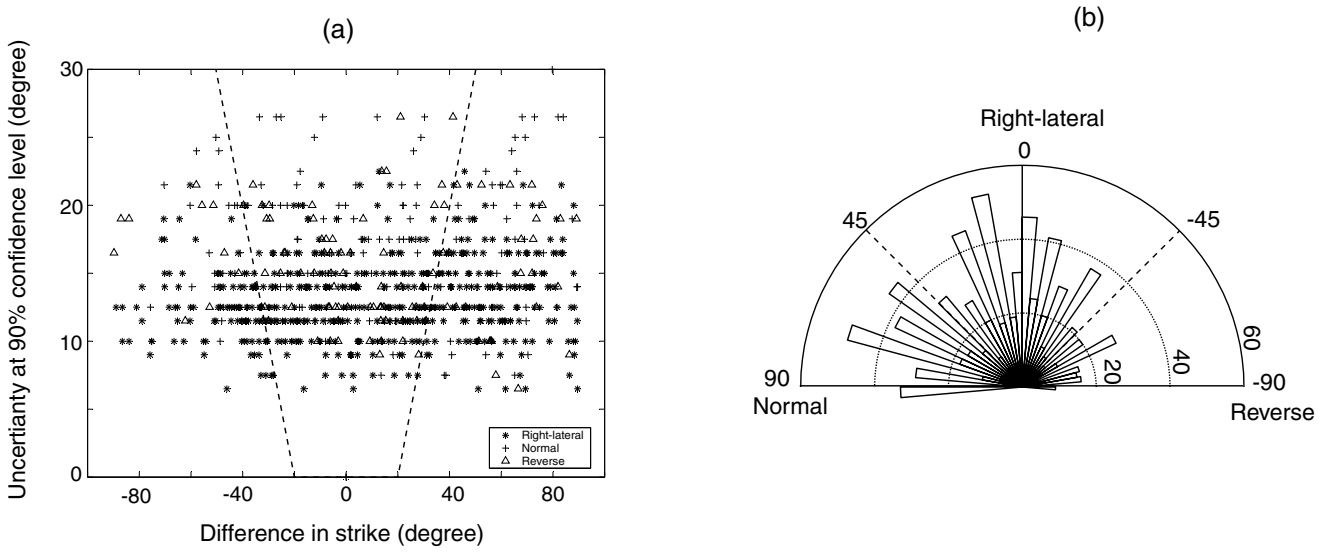

Figure 7. (a) The difference in strike of aftershock focal plane with that of the local mainshock fault is plotted against the uncertainty in strike of aftershock focal plane. We include only the 751 aftershocks that fall within 0.5 km of the mainshock rupture and have reliable first-motion solutions; 42% of these aftershocks are within 20° of the local strike at the 90% confidence level (those between the two dashed lines). (b) The histogram of the sense of motion (rake) on the chosen plane. Right-lateral refers to those that have a larger horizontal component than vertical.

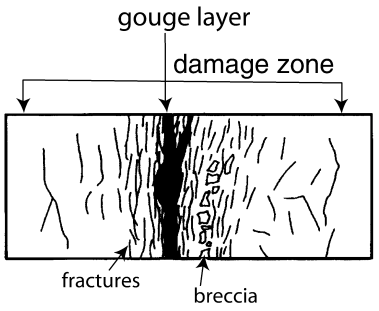

Figure 8. Schematic model of the gouge layer-damage zone morphology of a natural fault. It consists of a narrow gouge layer bounded by a broad damaged zone of subsidiary faults. The fracture density in the damage zone generally decreases with distance away from the center (modified from Wallace and Morris, 1986).

an entire fault zone are rare. Chester and Chester (1998) attempted to address this issue, however, in their study of the Punchbowl fault, an exhumed member of the San Andreas fault zone. They speculated that less than 100 m of the 40 km of dextral offset across the Punchbowl fault, a mere 0.25%, has been accommodated by faults outside of the 0.5-m-wide gouge layer.

How does this compare with deformation across the Landers mainshock and aftershock zone? For the mainshock rupture, we have a direct measure of slip on the surface traces of the faults. For the aftershocks, we must estimate slip indirectly, using the relationship between seismic moment and slip. We can calculate a hypothetical sum of aftershock slip, d, by using the conventional equation, $d = \Sigma M_0/(\mu A)$, where $\mu = 3.0 \times 10^{11}$ dyne/cm^2, ΣM_0 is the summed moment of aftershocks projected to their closest locations on the mainshock rupture planes, and A is the area of mainshock fault plane onto which the aftershocks are projected. We make the calculation for the Johnson Valley fault, because it is representative of the other principal faults of the rupture. The average slip on the Johnson Valley fault during the Landers mainshock was 2 m, and the nominal aftershock slip across the Johnson Valley fault averages about 1 cm. Thus, aftershock slip is about 0.5% of mainshock slip. This value is not all that different from the 0.25% value estimated by Chester and Chester (1998) for the ratio of slip across the Punchbowl gouge zone and the surrounding fault zone. Thus, it is plausible and even likely that the Landers aftershocks are merely the manifestation of a broad damage zone of small faults that extends out from narrow gouge zones that contain the principal ruptures of the mainshock.

What are the implications of adopting Chester and Chester's (1998) model of a fault zone for the Landers mainshock rupture and aftershock zone? Their observations, as well as others (Chester and Logan, 1986; Chester *et al.*, 1993; Schulz and Evans, 1998; Brune, 2001), show that the majority of displacement normally occurs in a band that ranges from a couple of meters to about 40 m in thickness. If displacements are accommodated by rupture during individual earthquakes, then this gouge layer, just a few tens of meters or less in width, is where mainshock rupture planes occur. Such gouge layers are 3 orders of magnitude narrower than the Landers aftershock cloud.

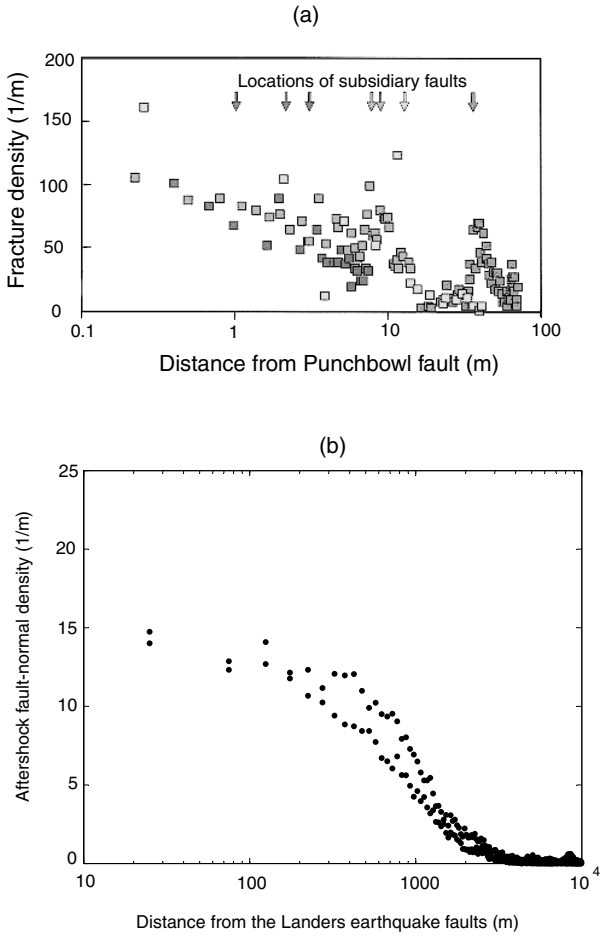

Figure 9. Density distributions of (a) mesoscopic fractures of the Punchbowl fault (Chester and Logan, 1986) and (b) Landers aftershocks as a function of distance normal to the principal fault plane. The fault-normal density of Landers aftershocks is summed over the entire length of the mainshock surface ruptures. The aftershock density at the center of the fault is 15 aftershocks per meter of distance perpendicular to the fault.

If we know the aftershock density within this gouge layer, then we can estimate how many aftershocks occurred within it. For the Landers rupture, Figure 9b shows that the aftershock density at the center of the fault is 15 aftershocks per meter of distance perpendicular to the fault, summed over the entire length of the ruptures. For gouge layers 2–40 m wide, this would yield just 30–600 aftershocks. This is equivalent to just 0.1%–2% of the total aftershock population. We have already shown that very few of the aftershocks occurred as reruptures of the mainshock rupture surfaces. This calculation suggests that in addition, very few of the aftershocks of the Landers earthquake occurred within the gouge layers associated with the main ruptures. Furthermore, if mainshock rupture only occurred on single or multiple discrete surfaces, rather than involving the entire gouge layer volume, the number of aftershocks falling on mainshock rupture planes would be even less.

But is the Landers aftershock sequence unusual? Recent improvements in locating earthquakes have revealed tighter clustering of aftershocks and clearer structural lineation of seismicity than could be resolved previously (e.g., Shearer, 1997; Shaw and Shearer, 1999; Fehler *et al.*, 2000; Richards-Dinger and Shearer, 2000; Rubin and Gillard, 2000; Waldhauser and Ellsworth, 2000). It is often observed that many aftershocks following major earthquakes appear to coincide with the parts of faults that slipped during the mainshock. However, it is still unclear that these tighter clusters of aftershocks occur on the same surfaces that moved in the mainshock or reflect activation of subsidiary faults in the surrounding volume. Although current earthquake-location technology does not enable resolution of individual aftershock locations to within or immediately outside of a mainshock rupture surface, geological observations provide important structural constraints that considerable percentages of aftershocks, if not most, must occur in the volume surrounding the zone of principal displacement. Exhumed fault zones show that there are numerous secondary fractures in the vicinity of the layer of fault gouge, with no or negligible offsets. These fractures quite plausibly originate during aftershocks.

Thus, rather than being an artifact of location error, the aftershock cloud may reflect a fundamental property of a fault zone. The discrete mainshock slip surfaces could appear remarkably planar, but cannot be perfectly or continuously planar. Geometric irregularities on the fault plane could give rise to locally large stresses and trigger off-fault aftershocks (Segall and Pollard, 1980; Das and Scholz, 1981). Structural complexities exist in all scales (e.g., Tchalenko, 1970; Aviles *et al.*, 1987; Okubo and Aki, 1987; Power *et al.*, 1987); meters-scale irregularities could be responsible for the aftershocks that are in the meters vicinity of mainshock rupture planes but in fact off-plane in the tabular surrounding volume. Hence, the characteristic complexity and network of faults of many sizes makes the wide distribution of aftershocks very likely. In this general sense, the Landers aftershock sequence is not that unusual.

To understand better the implications of these observations and hypotheses, we should distinguish at least five types of aftershocks, classifying them with respect to their locations relative to mainshock fault planes (Fig. 10). There are (1) class 1A aftershocks, those that occur on the same surfaces that slipped during the mainshock; and class 1B aftershocks, those occur in the gouge layer but off the planes that slipped during the mainshock; (2) class 2 aftershocks, those that occur on the same faults, but beyond the rupture termini of the mainshock; (3) class 3 aftershocks, those that occur on the subsidiary faults in the volume of damage zone surrounding the mainshock fault planes; and (4) class 4 aftershocks, remotely triggered aftershocks on faults farther from the principal faults of the mainshock rupture. Kisslinger (1996) proposed three similar classes of aftershocks, but combined our categories 1A, 1B, and 3 into a single category. Even though it might be beyond the limit of

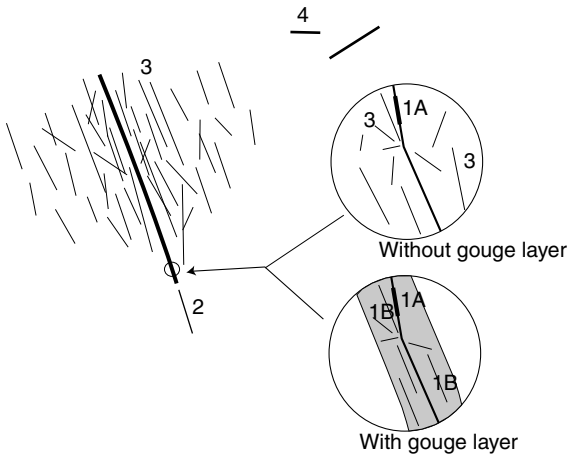

Figure 10. Schematic diagram illustrates the classification of aftershocks with respect to their locations relative to mainshock fault planes. See text for the definition for each class of aftershocks.

earthquake-location technology, the distinction between class 1B and 1A aftershocks is mechanically important, because they occur on different surfaces. Only class 1A aftershocks among all types represent truly the reruptures of the mainshock rupture plane. Although class 3 aftershocks appear to be the spatial extension of class 1B aftershocks into the bounding region, the distinction between class 1B and 3 aftershocks could also be significant. Class 1B aftershocks may in general have lower stress drops than class 3 aftershocks, if the gouge material will lower the frictional strength (Byerlee, 1978) than the surrounding medium and the boundary between the gouge layer and the surrounding host rock is general sharp (e.g., Chester and Logan, 1986; Cowan, 1999).

Perhaps aftershock sequences of major earthquakes are a combination of different classes, but the relative portion of each type varies among ruptures. In this article, we show that the Landers aftershock sequence has a small percentage of class 1 and 2 aftershocks. In contrast, Rubin and Gillard (2000) demonstrated that aftershocks of the earthquakes they studied occurred on the mainshock fault plane, but beyond the termini of the mainshock rupture. Thus, the aftershocks of the earthquakes in their study were predominantly class 2 aftershocks. Common in both studies, however, is that class 1A and 1B aftershocks are rare; aftershocks in Rubin and Gillard (2000) did not tend to occur on the parts of the faults that slipped during the mainshock, either.

The difference in manifestation of aftershock types may be due to factors such as the magnitude of the mainshock and the different degrees of geometric irregularity of the principal faults, or the cumulative slip of the fault if fault-trace complexity decreases with large cumulative slip (Wesnousky, 1988). The larger the mainshock magnitude is, the wider the aftershock cloud would be, if keeping all other parameters fixed. If the mainshock principal faults are geometrically more irregular or fragmented, then more aftershocks would be off-plane. For example, in Rubin and Gillard (2000), the earthquakes are microearthquakes and are located in the creeping section of the San Andreas fault. The wide Landers aftershock clouds may indicate the great complexity of the Landers principal faults.

An important implication of our analysis is that aftershock populations reveal the nature of the fractured medium around principal faults. This is consistent with another observation that higher *b*-values are associated with segments of mainshock rupture of more cracks. This is compatible with previous results that higher material heterogeneity or crack densities are associated with higher *b*-values for background seismicity (Mogi, 1962) and also in volcanic areas (Wyss *et al.*, 1997; Wiemer *et al.*, 1998). Thus, the ubiquitously observed Gutenberg–Richter power-law relationship of regional seismicity would not arise from the dynamics of failure of a single smooth and planar fault with particular frictional properties, as claimed in some numerical models (e.g., Burridge and Knopoff, 1967; Carlson and Langer, 1989; Langer *et al.*, 1996). *B*-value statistics would, instead, be a measure of the complexity of the broader fault zone or a network of faults (Wesnousky, 1994; Ben-Zion, 1996; Stirling *et al.*, 1996).

Conclusions

We have observed three things about the aftershock sequence of the 1992 Landers earthquake and its relationship to the ruptures of the mainshock. First, the aftershocks occur in a cloud surrounding the mainshock fault ruptures. But, this cloud is far too wide to be due to erroneously located events generated by rerupture of the mainshock rupture planes. This implies rupture of hundreds of secondary faults within a zone of failure that is kilometers in width.

Furthermore, the focal mechanisms of most of the aftershocks that originated close to the mainshock ruptures are inconsistent with generation by the mainshock ruptures. Less than a third of the aftershocks that are within half a kilometer of the mainshock rupture planes exhibited orientations and senses of motion consistent with the principal ruptures.

Finally, *b*-values are higher along those parts of the principal rupture where rupture complexity at the surface is greater. This further suggests that the aftershock population is controlled by the structure of the fault zone, rather than by the physical properties of the principal fault planes.

One important implication of this work is that the Gutenberg–Richter relationship that characterizes most seismic regions and most aftershock sequences reflects the population of faults in a region or within a broad fault zone, not the behavior of a planar active fault.

Acknowledgments

We thank A. Rubin, M. Fehler, and an anonymous reviewer for their constructive reviews of this article and K. Richards-Dinger and P. Shearer

for sharing their relocated Landers aftershock data set. Discussion with Eric Cowgill improved Figure 10. This research was supported by the Southern California Earthquake Center. SCEC was funded by NSF Cooperative Agreement EAR-8920136 and USGS Cooperative Agreements 14-08-0001-A0899 and 1434-HQ-97AG01718. This research was also partially supported by U.S. Geological Survey Grant 99HQGR0039 to Caltech. This article is Southern California Earthquake Center Contribution 635 and Caltech Seismological Laboratory Contribution Number 8855.

References

Aki, K. (1965). Maximum likelihood estimates of b in the formula $\log N = a - bM$ and its confidence limits, *Bull. Earthquake Res. Inst. Tokyo Univ.* **43,** 237–239.

Aviles, C. A., C. H. Scholz, and J. Boatwright (1987). Fractal analysis applied to characteristic segments of the San Andreas Fault, *J. Geophys. Res.* **92,** 331–344.

Ben-Zion, Y. (1996). Stress, slip, and earthquakes in models of complex single-fault systems incorporating brittle and creep deformations, *J. Geophys. Res.* **101,** 5677–5706.

Brune, J. N. (2001). Fault-normal dynamic unloading and loading: an explanation for "non-gouge" rock powder and lack of fault-parallel shear bands along the San Andreas fault, *EOS* **82,** F854.

Burridge, R., and L. Knopoff (1967). Model and theoretical seismicity, *Bull. Seism. Soc. Soc. Am.* **57,** 341–371.

Byerlee, J. D. (1978). Friction of rocks, *Pageoph* **116,** 615–626.

CDMG (California Department of Conservation, Division of Mines and Geology) (2000). Digital images of official maps of Alquist-Priolo earthquake fault zones of California, southern region, DMG CD 2000–003.

Carlson, J. M., and J. S. Langer (1989). Properties of earthquakes generated by fault dynamics, *Phys. Rev. Lett.* **62,** 2632–2635.

Chester, F. M., and J. S. Chester (1998). Ultracataclasite structure and friction processes of the Punchbowl fault, San Andreas system, California, *Tectonophysics* **295,** 199–221.

Chester, F. M., and J. M. Logan (1986). Implications for mechanical properties of brittle faults from observations of the Punchbowl Fault zone, California, *Pageoph* **124,** 79–106.

Chester, F. M., J. P. Evans, and R. L. Biegel (1993). Internal structure and weakening mechanisms of the San Andreas fault, *J. Geophys. Res.* **98,** 771–786.

Cowan, D. (1999). Do faults preserve a record of seismic slip? a field geologist's opinion, *J. Struct. Geology* **21,** 995–1001.

Das, S., and C. H. Scholz (1981). Off-fault aftershock clusters caused by shear stress increase? *Bull. Seism. Soc. Am.* **71,** 1669–1675.

Deng, J., M. Gurnis, H. Kanamori, and E. Hauksson (1998). Viscoelastic flow in the lower crust after the 1992 Landers, California, earthquake, *Science* **282,** 1689–1692.

Deng, J., K. Hudnut, M. Gurnis, and E. Hauksson (1999). Stress loading from viscous flow in the lower crust and triggering of aftershocks following the 1994 Northridge, California, earthquake, *Geophys. Res. Lett.* **26,** 3209–3212.

Dietz, L. D., and W. L. Ellsworth (1990). The October 17, 1989, Loma Prieta, California, earthquake and its aftershocks: geometry of the sequence from high-resolution locations, *Geophys. Res. Lett.* **17,** 1417–1420.

Fehler, M., and P. Johnson (1989). Determination of fault planes at Coalinga, California by analysis of patterns in aftershock locations, *J. Geophys. Res.* **94,** 7496–7506.

Fehler, M., W. S. Philips, L. House, R. H. Jones, R. Aster, and R. Charlotte (2000). Improved relative locations of clustered earthquakes using constrained multiple event location, *Bull. Seism. Soc. Am.* **71,** 775–780.

Freed, A., and J. Lin (1998). Time-dependent changes in failure stress following thrust earthquakes, *J. Geophys. Res.* **103,** 24,393–24,409.

Gomberg, J., and S. Davis (1996). Stress/strain changes and triggered seismicity following the M_w 7.3 Landers, California, earthquake, *J. Geophys. Res.* **101,** 751–764.

Hardebeck, J. L., J. J. Nazareth, and E. Hauksson (1998). The static stress change triggering model: constrains from two southern California aftershock sequences, *J. Geophys. Res.* **103,** 24,427–24,437.

Hauksson, E. (1994). State of stress from focal mechanisms before and after the 1992 Landers earthquake sequence, *Bull. Seism. Soc. Am.* **84,** 917–934.

Hauksson, E. (2000). Crustal structure and seismicity distribution adjacent to the Pacific and North America plate boundary in Southern California, *J. Geophys. Res.* **105,** 13,875–13,903.

Hauksson, E., and A. Michael (2001). Los Angeles seismotectonics: evidence from shotgun seismicity patterns and gridlock of Late Quaternary faults and folds, *EOS* **82,** no. 117, F829.

Hauksson, E., L. M. Jones, K. Hutton, and D. Eberphart-Phillips (1993). The 1992 Landers earthquake sequence: seismological observations. *J. Geophys. Res.* **98,** 19,835–19,858.

Hill, D. P., M. J. S. Johnston, J. O. Langbein, and R. Bilham (1995). Response of Long Valley caldera to the $M_w = 7.3$ Landers, California, earthquake, *J. Geophys. Res.* **100,** 12,985–13,005.

Hudnut, K. W., Y. Bock, M. Cline, P. Fang, Y. Feng, J. Freymueller, X. Ge, W. K. Gross, D. Jacksson, M. Kim, N. E. King, J. Langbein, S. C. Larsen, M. Lisowski, Z.-K. Shen, J. Svare, and J. Zhang (1994). Coseismic displacements of the 1992 Landers earthquake sequence, *Bull. Seism. Soc. Am.* **84,** 625–645.

Jennings, C. W. (1994). Fault activity map of California and adjacent areas, Department of Conservation; Division of Mines and Geology geologic map 6, scale 1:75,000.

Kanamori, H., and D. L. Anderson (1975). Theoretical basis of some empirical relations in seismology, *Bull. Seism. Soc. Am.* **65,** 1073–1096.

Kanamori, H., H.-K. Thio, D. Dreger, E. Hauksson, and T. Heaton (1992). Initial investigation of the Landers California earthquake of 28 June 1992 using TERRAscope, *Geophys. Res. Lett.* **19,** 2267–2270.

King, G. C. P., R. S. Stein, and J. Lin (1994). Static stress changes and the triggering of earthquakes, *Bull. Seism. Soc. Am.* **84,** 935–953.

Kisslinger, C. (1996). Aftershocks and fault-zone properties. *Adv. Geophys.* **38,** 1–36.

Langer, J. S., J. M. Carlson, C. R. Myers, and B. E. Shaw (1996). Slip complexity in dynamic models of earthquake faults, *Proc. Natl. Acad. Sci.* **93,** 3825–3829.

McGill, S. F., and C. M. Rubin (1999). Surficial slip distribution on the central Emerson fault during the June 28, 1992, Landers earthquake, California, *J. Geophys. Res.* **104,** 4811–4833.

Mendoza, C., and S. H. Hartzell (1988). Aftershock patterns and main shock faulting, *Bull. Seism. Soc. Am.* **78,** 1438–1449.

Mogi, K. (1962). Magnitude-frequency relation for elastic shocks accompanying fractures of various materials and some related problems in earthquakes, *Bull. Earthquake Res. Inst. Tokyo Univ.* **40,** 831–853.

Mori, J., and R. Abercrombie (1997). Depth dependence of earthquake frequency-magnitude distributions in California: implications for the rupture initiation, *J. Geophys. Res.* **102,** 15,081–15,090.

Nakamura, M., and M. Ando (1996). Aftershock distribution of the January 17, 1995 Hyogo-ken earthquake determined by the JHD method, *J. Phys. Earth* **44,** 329–335.

Okubo, P., and K. Aki (1987). Fractal geometry in the San Andreas Fault system, *J. Geophys. Res.* **92,** 345–355.

Power, W. L., T. E. Tullis, S. R. Brown, G. N., Boitnott, and C. H. Scholz (1987). Roughness of natural fault surfaces, *Geophys. Res. Lett.* **14,** 29–32.

Resenberg, P., and D. H. Oppenheimer (1985). FPFIT, FPLOT, and FPPAGE: Fortran computer programs for calculating and displaying earthquake fault-plane solutions, *U.S. Geol. Surv. Open-File Rept. OF 85-0739*, 109.

Reasenberg, P. A., and R. W. Simpson (1992). Response of regional seismicity to the static stress change produced by the Loma Prieta earthquake, *Science* **255,** 1687–1690.

Richards-Dinger, K. B., and P. M. Shearer (2000). Earthquake locations in southern California obtained using source-specific station terms, *J. Geophys. Res.* **105,** 10,939–10,960.

Rubin, A. M., and D. Gillard (2000). Aftershock asymmetry/rupture directivity among central San Andreas fault microearthquakes, *J. Geophys. Res.* **105,** 19,095–19,109.

Schulz, S. E., and J. P. Evans (1998). Spatial variability in microscopic deformation and composition of the Punchbowl fault, southern California: implications for mechanisms, fluid-rock interaction, and fault morphology, *Tectonophysics* **295,** 223–244.

Segall, P., and D. D. Pollard (1980). Mechanics of discontinuous faults, *J. Geophys. Res.* **85,** 4337–4350.

Shaw, J. H., and P. M. Shearer (1999). An elusive blind-thrust fault beneath metropolitan Los Angeles, *Science* **283,** 1516–1518.

Shearer, P. (1997). Improving local earthquake locations using the L1 norm and waveform cross correlation: application to the Whittier Narrow, California, aftershock sequence, *J. Geophys. Res.* **102,** 8269–8283.

Sieh, K. E., L. Jones, E. Hauksson, K. Hudnut, D. Eberhart-Phillips, T. Heaton, S. Hough, K. Hutton, H. Kanamori, A. Lijie, S. Lindvall, S. F. McGill, J. Mori, C. Rubin, J. A. Spotila, J. Stock, H. K. Thio, J. Treiman, B. Wernicke, and J. Zachariasen (1993). Near-field investigations of the Landers earthquake sequence, April to July, 1992, *Science* **260,** 171–176.

Stein, R. S., and M. Lisowski (1983). The 1979 Homestead Valley earthquake sequence, California: control of aftershocks and postseismic deformation, *J. Geophys. Res.* **88,** 6477–6490.

Stein, R. S., G. C. P. King, and J. Lin (1994). Stress triggering of the 1994 $M = 6.7$ Northridge, California earthquake by its predecessors, *Science* **265,** 1432–1435.

Stirling, M. W., S. G. Wesnousky, and K. Shimazaki (1996). Fault trace complexity, cumulative slip, and the shape of the magnitude-frequency distribution for strike-slip faults: a global survey, *Geophys. J. Int.* **124,** 833–868.

Spotila, J. A., and K. Sieh (1995). Geologic investigations of a "slip gap" in the surficial ruptures of the 1992 Landers earthquake, southern California, *J. Geophys. Res.* **100,** 534–559.

Tchalenko, J. S. (1970). Similarities between shear zones of different magnitudes, *Bull. Geol. Soc. Am.* **81,** 1625–1640.

USGS/CDMG (United States Geological Survey/California Divisions of Mines and Geology Staff) (1992). Pattern of surface ruptures associated with the June 28, 1992, Landers earthquake (abstract). *Trans. Am. Geophys. Union* **73,** 357–358.

Waldhauser, F., and W. L. Ellsworth (2000). A double-difference earthquake location algorithm: method and application to the northern Hayward Fault, California, *Bull. Seism. Soc. Am.* **90,** 1353–1368.

Wald, D. J., and T. H. Heaton (1994). Spatial and temporal distribution of slip for the 1992 Landers, California, earthquake, *Bull. Seism. Soc. Am.* **84,** 668–691.

Wallace, E. W., and H. T. Morris (1986). Characteristic of faults and shear zones in deep mines, *Pageoph* **124,** 107–125.

Wesnousky, S. G. (1988). Seismological and structural evolution of strike-slip faults, *Nature* **335,** 340–342.

Wesnousky, S. G. (1994). The Gutenberg-Richter or characteristic earthquake distribution, which is it? *Bull. Seism. Soc. Am.* **84,** 1940–1959.

Wiemer, S., and K. Katsumata (1999). Spatial variability of seismicity parameters in aftershock zones, *J. Geophys. Res.* **104,** 13,135–13,151.

Wiemer S., S. R. McNutt, and M. Wyss (1998). Temporal and three-dimensional spatial analysis of the frequency-magnitude distribution near Long Valley Caldera, California, *Geophys. J. Int.* **134,** 409–421.

Wyss, M., K. Shimazaki, and S. Wiemer (1997). Mapping active magma chambers by *b* value beneath Off-Izu volcano, Japan, *J. Geophys. Res.* **102,** 20,413–20,433.

Zachariasen, J., and K. E. Sieh (1995). The transfer of slip between en echelon strike-slip faults: a case study from the 1992 Landers earthquake, southern California, *J. Geophys. Res.* **100,** 15,281–15,301.

Seismological Laboratory and
Division of Geological and Planetary Sciences 100-23
California Institute of Technology
Pasadena, California 91125
(L.J., K.S., E.H.)

Manuscript received 26 February 2002.